Progress In Electromagnetics Research M, Vol. 32, 1–11, 2013

MULTIRESOLUTION TIME DOMAIN SCHEME USING SYMPLECTIC INTEGRATORS

Zheng Sun*, Li Hua Shi, Xiang Zhang, and Ying Hui Zhou

National Key Laboratory on Electromagnetic Environmental Effects and Electro-optical Engineering, PLA University of Science and Technology, Nanjing, Jiangsu 210007, China

Abstract—We incorporate high-order symplectic time integrators into multiresolution time domain (MRTD) schemes. The stability and numerical dispersion analysis are presented. The proposed scheme preserves the symplectic structure of Maxwell's equations and can be easily implemented in program codes. Compared to Runge-Kutta (RK)-MRTD, the suggested scheme is more accurate in long-term simulations and requires less computational resource.

1. INTRODUCTION

The symplectic integrator was originally developed to solve numerical systems derived from a Hamiltonian formulation. It preserves the symplectic structure of the phase space, and as a result, it can conserve the total system's energy (i.e., non-dissipative) [1]. This property is very suitable for the long-term integration of the system. As the Maxwell's equations can be treated as a Hamiltonian system, some researchers adopted symplectic integrators for use in computational electromagnetics (CEM) in recent years. Hirono et al. [2], Sha et al. [3–5] and Kusaf et al. [6] have done lots of work on combining this method with the FDTD scheme, and have got excellent results.

As an alternative method to the conventional FDTD [7–9] scheme, the multiresolution time domain (MRTD) [10, 11] shows highly linear dispersion characteristics. Therefore, it can use much coarser grids without sacrificing computational precision. Most MRTD schemes

Received 7 May 2013, Accepted 6 July 2013, Scheduled 15 July 2013

* Corresponding author: Zheng Sun (sunzheng08005405@163.com).

employ high-order special finite differences, but they still produce second-order error convergence as long as they are coupled with the second-order accurate leap-frog time integration [12]. To overcome this problem, Cao et al. proposed RK-MRTD scheme [13, 14], which employs the Runge-Kutta method to get high-order accuracy in time. However, the RK-MRTD scheme destroys the symplectic structure of Maxwell's equations (dissipative) and requires 2.5 (7/3 in 2D case) times memory of that of the traditional MRTD in three dimensions.

In this paper, we incorporate symplectic integrators into MRTD. This is implemented by discretizing the Maxwell's equations with symplectic scheme in time and MRTD scheme in space. The proposed scheme is non-dissipative and explicit, which only requires the same storage as the traditional MRTD. Compared to RK-MRTD, the suggested scheme is more accurate and consumes less computational resource.

2. SCHEMES

2.1. Maxwell's Equations

Maxwell's curl equations in homogeneous, lossless and sourceless medium can be written as:

$$\frac{\partial \mathbf{H}}{\partial t} = -\mu^{-1}\nabla \times \mathbf{E} \ , \quad \frac{\partial \mathbf{E}}{\partial t} = \varepsilon^{-1}\nabla \times \mathbf{H} \tag{1}$$

which can be expanded into six scale equations. μ and ε are the permeability and permittivity, respectively.

2.2. MRTD in Spatial Discretization

Here we expand the electromagnetic fields with scaling functions only in space, while let the actual wavelet coefficients be functions of time, which are to be determined [13]. For simplicity, we take only Ex as an example, other components can be represented in a similar form.

$$E_x(\vec{r}, t) = \sum_{i,j,k=-\infty}^{+\infty} E(t)^{\phi x}_{i+1/2,j,k} \phi_{i+1/2}(x)\phi_j(y)\phi_k(z) \tag{2}$$

where, i, j, and k denote the discrete space indexes related to the space via $x = i\Delta x$, $y = j\Delta y$, $z = k\Delta z$, Δx, Δy and Δz indicate the discretization intervals. The function ϕ is the scaling function.

$$\phi_m(s) = \phi(s/\Delta s - m) \quad s = x, y, z \tag{3}$$

Substituting the expansions into Maxwell's six scalar equations, we obtain (just present two for simplicity):

$$\begin{aligned}
&\frac{\partial E^{\phi x}_{i+1/2,j,k}(t)}{\partial t}\\
&= \varepsilon^{-1} \sum_{v=-ns}^{ns-1} a(v)\Big(H^{\phi z}_{i+1/2,j+v+1/2,k}(t)/\Delta y - H^{\phi y}_{i+1/2,j,k+v+1/2}(t)/\Delta z\Big)\\
&= \varepsilon^{-1}\left(LyH^{\phi}_{z} - LzH^{\phi}_{y}\right) \qquad (4a)\\
&\frac{\partial H^{\phi x}_{i,j+1/2,k+1/2}(t)}{\partial t}\\
&= -\mu^{-1} \sum_{v=-ns}^{ns-1} a(v)\Big(E^{\phi z}_{i,j+v+1,k+1/2}(t)/\Delta y - E^{\phi y}_{i,j+1/2,k+v+1}(t)/\Delta z\Big)\\
&= -\mu^{-1}\left(LyE^{\phi}_{z} - LzE^{\phi}_{y}\right) \qquad (4b)\\
L_i &= \sum_{v=-ns}^{ns-1} a(v)/\Delta i, \quad i = x, y, z \qquad (4c)
\end{aligned}$$

where ns, called 'stencil size', represents the effective support of the basis function. $a(v)$ are the connection coefficients, decided by the basis functions [10]. The rest equations can be derived in a similar way. Now we can write the Maxwell's equations symbolically as:

$$\frac{\partial}{\partial t}\begin{pmatrix}\mathbf{H}^{\phi}\\ \mathbf{E}^{\phi}\end{pmatrix} = (\mathbf{A}+\mathbf{B})\begin{pmatrix}\mathbf{H}^{\phi}\\ \mathbf{E}^{\phi}\end{pmatrix} \qquad (5)$$

with

$$\mathbf{A}=\begin{pmatrix}\mathbf{0}_{3\times3} & -\mu^{-1}\mathbf{L}\\ \mathbf{0}_{3\times3} & \mathbf{0}_{3\times3}\end{pmatrix},\ \mathbf{B}=\begin{pmatrix}\mathbf{0}_{3\times3} & \mathbf{0}_{3\times3}\\ \varepsilon^{-1}\mathbf{L} & \mathbf{0}_{3\times3}\end{pmatrix},\ \mathbf{L}=\begin{pmatrix}0 & -Lz & Ly\\ Lx & 0 & -Lx\\ -Ly & Lx & 0\end{pmatrix} \qquad (6)$$

2.3. Symplectic Scheme in Temporal Discretization

As to (5), the evolution of the electromagnetic field during the time-step Δt can be exactly expressed by the exponential operator [2]:

$$\left.\begin{pmatrix}\mathbf{H}^{\phi}\\ \mathbf{E}^{\phi}\end{pmatrix}\right|_{\Delta t} = \exp(\Delta t(\mathbf{A}+\mathbf{B}))\left.\begin{pmatrix}\mathbf{H}^{\phi}\\ \mathbf{E}^{\phi}\end{pmatrix}\right|_{0} \qquad (7)$$

Using the symplectic integrator propagator technique [2], the evolution matrix $\exp(\Delta t(\mathbf{A}+\mathbf{B}))$ can be presented as:

$$\exp(\Delta t(\mathbf{A}+\mathbf{B})) = \prod_{l=1}^{m}(\mathbf{I}_6 + c_l\Delta t\mathbf{A})(\mathbf{I}_6 + d_l\Delta t\mathbf{B}) + O\left((\Delta t)^{p+1}\right) \qquad (8)$$

where c_l, d_l are the symplectic integrators. m and p are the stage number and order of the propagator respectively ($m \geqslant p$). Then, (7) can be written approximately as:

$$\left.\begin{pmatrix}\mathbf{H}^{\phi}\\ \mathbf{E}^{\phi}\end{pmatrix}\right|_{\Delta t} = \left(\prod_{l=1}^{m}(\mathbf{I}_6 + c_l\Delta t\mathbf{A})(\mathbf{I}_6 + d_l\Delta t\mathbf{B})\right)\left.\begin{pmatrix}\mathbf{H}^{\phi}\\ \mathbf{E}^{\phi}\end{pmatrix}\right|_{0} \tag{9}$$

As can be seen, this is an explicit symplectic integrator which can be easily implemented.

2.4. MRTD Using Symplectic Integrators

According to the derivations above, we get the symplectic MRTD. As to the lth-stage in a m-stage scheme, the expressions of $E^{\phi x}$, $H^{\phi x}$ are as follows:

$$\begin{aligned}{}_{n+l/m}E^{\phi x}_{i+1/2,j,k} = {}&{}_{n+(l-1)/m}E^{\phi x}_{i+1/2,j,k} + (d_l\Delta t/\varepsilon)\cdot\sum_{v=-ns}^{ns-1}a(v)\\ &\left({}_{n+(l-1)/m}H^{\phi z}_{i+1/2,j+v+1/2,k}/\Delta y - {}_{n+(l-1)/m}H^{\phi y}_{i+1/2,j,k+v+1/2}/\Delta z\right)\end{aligned} \tag{10a}$$

$$\begin{aligned}{}_{n+l/m}H^{\phi x}_{i,j+1/2,k+1/2} = {}&{}_{n+(l-1)/m}H^{\phi x}_{i,j+1/2,k+1/2} - (c_l\Delta t/\mu)\cdot\sum_{v=-ns}^{ns-1}a(v)\\ &\left({}_{n+(l-1)/m}E^{\phi z}_{i,j+v+1,k+1/2}/\Delta y - {}_{n+(l-1)/m}E^{\phi y}_{i,j+1/2,k+v+1}/\Delta z\right)\end{aligned} \tag{10b}$$

One can note that this scheme requires the same memory as the traditional MRTD.

3. STABILITY AND DISPERSION

3.1. Stability

It is well known that the explicit numerical scheme is limited by the Courant-Friedrich-Levy (CFL) condition, that is:

$$\Delta t \leq \alpha(\Delta s/v_c) \tag{11}$$

α is the CFL number, and the maximum α can be solved as [3]:

$$\alpha_{\max} = \lambda_T/\lambda_S \tag{12}$$

where λ_T is the temporal stability factor and λ_S the special stability factor. As for MRTD, λ_S is given by:

$$\lambda_S = \sqrt{\dim}\sum_{v=-ns}^{ns-1}|a(v)| \tag{13}$$

dim is the dimension number.

In this paper, we employ the Daubechies scaling functions as bases, which are compactly supported and shifted interpolation [15]. Dn is the Daubechies scaling functions with n vanishing moments. The nonzero coefficients $a(v)$ of the Daubechies scaling functions are given in Table 1.

Table 1. The nonzero coefficients $a(v)$ of the Daubechies scaling functions Dn, $a(v) = -a(1-v)$ for $v < 0$.

	D2	D3
$a(0)$	1.229166666	1.2918129281
$a(1)$	−0.0937500000	−0.1371343465
$a(2)$	0.0104166667	0.0287617723
$a(3)$		−0.0034701413
$a(4)$		0.0000080265
λ_S	4.6188	5.0617

λ_T can be obtained by solving the condition [2]:

$$|\gamma| = \left|1 + \left(\frac{1}{2}\right) \sum_{p=1}^{m} g_p \left\{v_c^2 \Delta_t^2 \left(\eta_x^2 + \eta_y^2 + \eta_z^2\right)\right\}^p\right| \leq 1 \tag{14a}$$

$$g_p = \sum_{1 \leq i_1 \leq j_1 < i_2 \leq j_2 < \ldots < i_p \leq j_p \leq m} c_{i_1} d_{j_1} c_{i_2} d_{j_2} \ldots c_{i_p} d_{j_p} + \sum_{1 \leq i_1 < j_1 \leq i_2 < j_2 \leq \ldots \leq i_p < j_p \leq m} d_{i_1} c_{j_1} d_{i_2} c_{j_2} \ldots d_{i_p} c_{j_p} \tag{14b}$$

$$\eta_i = \sum_{v=0}^{ns-1} a(v) \left(e^{-j(v+1/2)ki\Delta i} - e^{j(v+1/2)ki\Delta i}\right) / \Delta i, \quad i = x, y, z \tag{14c}$$

Usually, we optimize the c_l, d_l to get the maximum λ_T. And for the time-reversible symplectic integrators: $c_l = c_{m-l+1}$, $d_l = d_{m-l}$, $(1 \leq l \leq m-1)$, and $d_m = 0$. The optimized coefficients c_l, d_l for 4-stage, 3-order and 5-stage, 4-order schemes are listed in Table 2 [3, 4].

Table 3 shows the maximum CFL number ($\alpha_{\max}$) of different symplectic MRTD (p, Dn) schemes, calculated by (12). p is the order of the symplectic integrators in time. Dn is the Daubechies scaling function employed in space.

Table 2. The optimized coefficients c_l, d_l for different symplectic integrators.

	4-stage, 3-order	5-stage, 4-order
c_1	0.81431188	0.16537923
c_2	−0.31431188	1.35491814
c_3		−2.04059474
d_1	−0.09376908	0.51541261
d_2	1.187538164	−0.01541261
λ_T	4.564	3.467

Table 3. The CFLmax of different schemes MRTD (p, Dn) for 3D case.

MRTD (p, Dn)	(2, D2)	(3, D2)	(4, D2)	(2, D3)	(3, D3)	(4, D3)
$\alpha_{\max}$	0.433	0.988	0.751	0.395	0.902	0.685

3.2. Dispersion

Due to the discretization in time and space, the numerical phase velocity in MRTD can differ from the vacuum speed of light, varying with the modal wavelength, the direction of propagation, and the grid size. Therefore, a nonphysical dispersion is introduced and affects the accuracy limits of simulations.

The radian frequency ω of the numerical mode is expressed as [2, 14]:

$$\omega = \arccos(\gamma)/\Delta t \tag{15}$$

Substituting the following relations, $\omega = 2\pi c/\lambda_c$, $k_x = k_p \sin(\theta)\cos(\phi)$, $k_y = k_p \sin(\theta)\sin(\phi)$, $k_z = k_p \cos(\theta)$, $k_p = 2\pi/\lambda_p$, $ppw = \lambda_c \Delta s/c$, $\Delta t = \alpha \Delta s/c$ into (15), we can obtained a function of variables ppw, λ_p, θ, ϕ and α, where ppw is the number of cells per wavelength; λ_c is the theoretical wavelength in the continuous medium; λ_p is the numeric wavelength; θ and ϕ are the elevation angle and the azimuth angle, respectively.

We assess the linear numerical dispersion performance by the relative phase velocity error:

$$\text{Error} = 20 \log_{10} |(v_p - v_c)/v_c| \tag{16}$$

Figures 1 and 2 show the relative phase velocity error versus the cell number per wavelength and angle ϕ, respectively. From Figs. 1 and 2, we can found that MRTD (2, D2) and MRTD (2, D3) show the worst performance, which is caused by their low-order time-stepping

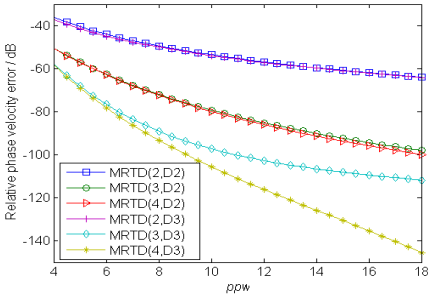

Figure 1. Relative phase velocity error versus the cell number per wavelength ($\theta = 60°$, $\phi = 45°$ and $\alpha = 0.35$).

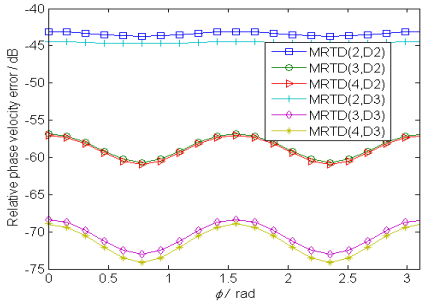

Figure 2. Relative phase velocity error versus angle ϕ. ($\theta = 60°$, $ppw = 6$ and $\alpha = 0.35$).

procedure. As the order of temporal discretization increases, MRTD (3, D2) and MRTD (3, D3) both get better performance than MRTD (2, D2) and MRTD (2, D3), respectively. However, MRTD (4, D2) doesn't show much improvement to MRTD (3, D2), while MRTD (4, D3) still obtains better performance than MRTD (3, D3). This means that the orders of accuracy in time and space should match to each other. As for MRTD based on D2, 3rd-order in time is enough. The higher order does not pay off dispersion-wise.

4. NUMERICAL RESULTS

4.1. 1D Propagation

Firstly, we consider a Gaussian pulse traveling in 1-D free space. The domain of simulation is 20 m. The Gaussian pulse, excited at the center, is described as $\exp(-4\pi((t - t_0)/\tau)^2)$, where $\tau = 100$ ps and $t_0 = 120$ ps. The time-domain waveforms along x-axis calculated by deferent schemes are recorded in Fig. 3 after the pulse traveling 300 ps. Table 4 shows the computing cost of different schemes. As we can see, MRTD (3, D2) agrees well with the analytical solution and remains stable and accurate, even with a larger spatial step and CFL. However, MRTD (2, D2) causes deviation in the waveform. And the attenuation of the amplitude of RK-MRTD (3, D2) is obvious. As to the computational cost, MRTD (3, D2) only consumes 40% memory and 23.6% CPU time of RK-MRTD (3, D2).

4.2. Resonant Frequencies of Rectangular Waveguide Cavity

We consider a three-dimensional air-filled cavity (2 m × 2 m × 1 m), which is excited at (1 m, 1 m, 0.5 m) while sampled at (0.5 m, 0.5 m,

Table 4. The computing cost of different schemes.

Schems	Δs (mm)	CFL	Number of iterations	Memory (KB)	CPU time (s)
MRTD (2, D2)	0.5	0.667	27000	156.3	8.94
MRTD (3, D2)	1	1	9000	156.3	3.37
RK-MRTD (3, D2)	1	0.625	14400	390.8	14.28

Note: Intel (R) CoreTM i5-3210M CPU@2.50 GHz.

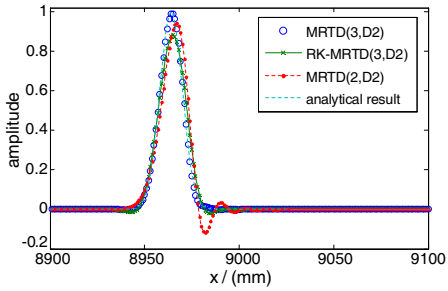

Figure 3. The waveforms along x-axis calculated by deferent schemes after the pulse propagating 300 ps.

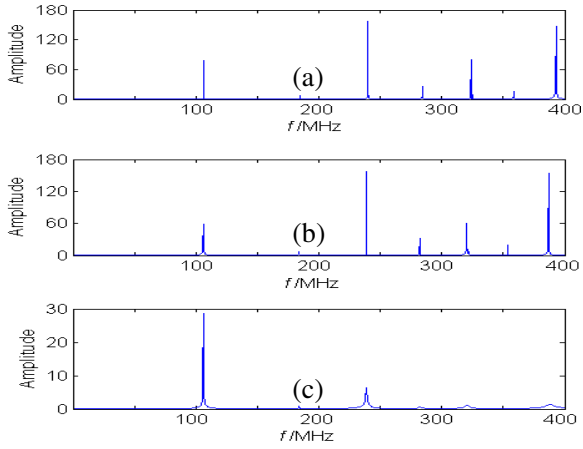

Figure 4. The frequency spectrums obtained by different schemes. (a) MRTD (2, D2), (b) MRTD (3, D2), (c) RK-MRTD (3, D2).

Table 5. The resonant frequencies calculated by different schemes.

Analytical Values (MHz)	MRTD (2, D2)	RK-MRTD (3, D2)	MRTD (3, D2)
106.07	106.2	106.0	106.0
183.71	184.6	184.0	184.0
237.17	240.0	238.8	238.6
280.62	284.4	282.2	282.0
318.20	323.8	321.0	320.4
351.78	358.6	356.0	353.8
382.43	393.0	388.4	386.8

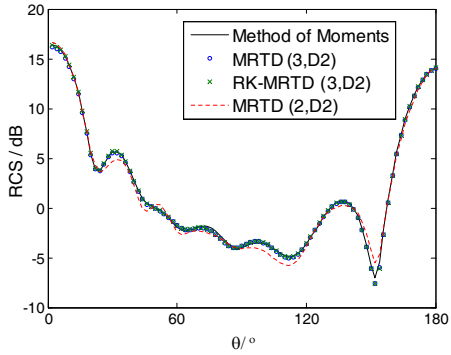

Figure 5. RCSs of a rectangular PEC cylinder obtained by different schemes.

0.5 m). The space step is $\Delta s = \Delta x = \Delta y = \Delta z = 0.25$ m, and the time step is $\Delta t = 0.25$ ns. The simulation runs for 20000 time steps. We calculate its resonant frequencies using MRTD (2, D2), MRTD (3, D2), RK-MRTD (3, D2), respectively.

The frequency spectrums calculated by different schemes are shown in Fig. 4. Table 5 lists some results for the resonant frequencies. We can see that RK-MRTD (3, D2) and MRTD (3, D2) are more accurate than MRTD (2, D2), meanwhile, MRTD (3, D2) is more accurate than RK-MRTD (3, D2). The amplitude of the frequency spectrums of RK-MRTD (3, D2) is smaller, which is due to its dissipative attenuation. And with the frequency increasing, the dissipative attenuation becomes more and more serious.

4.3. RCS of a Rectangular PEC Cylinder

Finally, we study the radar cross section (RCS) for a rectangular perfectly electric conducting PEC cylinder with cross-section dimensions

of $0.02\,\mathrm{m} \times 0.02\,\mathrm{m}$, which is equivalent to $2\lambda \times 2\lambda$ (λ is the wavelength of the excitation sinusoidal pulse). For every scheme, the spatial discretization is $\lambda/10$ and the CFL $= 0.5$. The incident wave is TM wave, and normal to the left side of the cylinder. The RCSs (normalized by λ) of the cylinder derived from the different algorithms are shown in Fig. 5. The results of MRTD (3, D2) and RK-MRTD (3, D2) is identical to that of method of moments (MoM), while the result of MRTD (2, D2) shows some obvious deviations.

5. CONCLUSIONS

In this paper, we incorporate high-order symplectic time integrators into MRTD schemes. Theoretically, by choosing proper discretizing orders in time and space, the proposed scheme can achieve desirable stability and linear dispersion properties. The symplectic MRTD keeps the symplectic structure of Maxwell's equations (non-dissipative) and can be easily implemented in program codes. Compared to RK-MRTD, the suggested scheme requires less computational resource and is more accurate for long-term simulations.

ACKNOWLEDGMENT

This work was supported by NCET and NSFC of China under Grant No. 07-0383 and No. 51077133, respectively. The authors also would like to thank the reviewers for helpful remarks.

REFERENCES

1. Sanz-Serna, J. M. and M. P. Calvo, *Numerical Hamiltonian Problems*, Chapman & Hall, London, UK, 1994.
2. Hirono, T., W. Lui, S. Seki, and Y. Yoshikuni, "A three-dimensional fourth-order finite-difference time-domain scheme using a symplectic integrator propagator," *IEEE Trans. on Microw. Theory and Tech.*, Vol. 49, 1640–1648, 2001.
3. Sha, W., Z. Huang, M. Chen, and X. Wu, "Survey on symplectic finite-difference time-domain scheme for Maxwell's equation," *IEEE Trans. on Antennas and Propag.*, Vol. 56, No. 2, 493–500, 2008.
4. Sha, W., Z. Huang, X. Wu, and M. Chen, "Application of the symplectic finite-difference time-domain scheme to electromagnetic simulation," *J. Comput. Phys.*, Vol. 225, 33–50, 2007.

5. Sha, W., X. Wu, Z. Huang, and M. Chen, "Waveguide simulation using the high-order symplectic finite-difference time-domain scheme," *Progress In Electromagnetics Research B*, Vol. 13, 237–256, 2009.
6. Kusaf, M., A. Y. Oztoprak, and D. S. Daoud, "Optimized exponential operator coefficients for symplectic FDTD method," *IEEE Microw. Wireless Compon. Lett.*, Vol. 15, No. 2, 86–88, 2005.
7. Gradoni, G., V. Mariani Primiani, and F. Moglie, "Reverberation chamber as a multivariate process: FDTD evaluation of correlation matrix and independent positions," *Progress In Electromagnetics Research*, Vol. 133, 217–234, 2013.
8. Izadi, M., M. Z. A. Ab Kadir, and C. Gomes, "Evaluation of electromagnetic fields associated with inclined lightning channel using second order FDTD-hybrid methods," *Progress In Electromagnetics Research*, Vol. 117, 209–236, 2011.
9. Vaccari, A., A. Cala' Lesina, L. Cristoforetti, and R. Pontalti, "Parallel implementation of a 3D subgridding FDTD algorithm for large simulations," *Progress In Electromagnetics Research*, Vol. 120, 263–292, 2011.
10. Krumpholz, M. and L. P. B. Katehi, "MRTD: New time-domain schemes based on multiresolution analysis," *IEEE Trans. on Microwave Theory and Tech.*, Vol. 44, No. 4, 555–571, 1996.
11. Liu, Y., Y.-W. Chen, P. Zhang, and X. Xu, "Implementation and application of the spherical MRTD algorithm," *Progress In Electromagnetics Research*, Vol. 139, 577–597, 2013.
12. Sarris, C. D., "New concepts for the multiresolution time domain (MRTD) analysis of microwave structures," *Proc. 34th Eur. Microw. Conf.*, Vol. 2, 881–884, London, UK, 2004.
13. Cao, Q., R. Kanapady, and F. Reitich, "High-order Runge-Kutta multiresolution time-domain methods for computational electromagnetics," *IEEE Trans. on Microw. Theory and Tech.*, Vol. 54, No. 8, 3316–3326, 2006.
14. Chen, X. and Q. Cao, "Analysis of characreristics of two-dimensional Runge-Kutta multiresolution time-domain scheme," *Progress In Electromagnetics Research M*, Vol. 13, 217–227, 2010.
15. Fujii, M. and W. J. R. Hoefer, "Dispersion of time-domain wavelet-Galerkin method based on Daubechies compactly supported scaling functions with three and four vanishing moments," *IEEE Microwave Guided Wave Lett.*, Vol. 10, No. 4, 125–127, 2000.